JOURNAL OF MICROENCAPSULATION
https://doi.org/10.1080/02652048.2023.2167011

Taylor & Francis
Taylor & Francis Group

RESEARCH ARTICLE

Polymer drug conjugates containing memantine, tacrine and cinnamic acid: promising nanotherapeutics for the treatment of Alzheimer's disease

Tobeka Naki[a], William Morwa Reagile Matshe[b], Mohammed Olusegun Balogun[b], Suprakas Sinha Ray[c], Samuel Ayodele Egieyeh[d] and Blessing Atim Aderibigbe[a]

[a]Department of Chemistry, University of Fort Hare, Alice, South Africa; [b]Polymer and Composites, CSIR Materials Science and Manufacturing, Pretoria, South Africa; [c]DST/CSIR National Centre for Nanostructured Materials, Council for Scientific and Industrial Research, Pretoria, South Africa; [d]School of Pharmacy, University of the Western Cape, Bellville Cape Town

ABSTRACT

Aim: To prepare polymer-drug conjugates containing a combination of memantine, tacrine, and *E*)-*N*-(3-aminopropyl)cinnamide, promising therapeutics for the treatment of neurodegenerative disorders.

Methods: The conjugates were characterised by ^{1}HNMR, particle size analysis, SEM, LC-MS, TEM/EDX, and XRD, followed by *in vitro* anti-acetylcholinesterase and drug release studies.

Results: ^{1}H NMR analysis revealed successful drug conjugation with drug mass percentages in the range of 1.3–6.0% w/w. The drug release from the conjugates was sustained for 10 h in the range of 20–36%. The conjugates' capability to inhibit acetylcholinesterase (AChE) activity was significant with IC_{50} values in the range of 13–44.4 μm which was more effective than tacrine (IC_{50} =1698.8 μm). The docking studies further confirmed that the conjugation of the drugs into the polymer improved their anti-acetylcholinesterase activity.

Conclusion: The drug release profile, particle sizes, and *in vitro* studies revealed that the conjugates are promising therapeutics for treating neurodegenerative disorders.

ARTICLE HISTORY
Received 9 July 2022
Accepted 4 January 2023

KEYWORDS
Alzheimer's disease; polymer-drug conjugate; memantine; tacrine; polyamidoamine; cinnamic acid

1. Introduction

Alzheimer's disease (AD) is characterised by the loss of cognitive function and a progressive loss of episodic memory which leads to impaired visuospatial skills and language as well as behavioural abnormalities, such as aggression, depression, and apathy (Fan *et al.* 2019, Zhang *et al.* 2021a). It is the world's sixth major cause of death and the most common cause of dementia (Haque and Levey 2019). Currently, over 50 million people suffer from AD globally, and this number is predicted to increase to 152 million by 2050 (Breijyeh and Karaman 2020). The shortage of effective treatment options results from the lack of sufficient knowledge about the actual pathology and process behind AD (Kuo and Rajesh 2019). Moreover, there is no cure for AD and there is a pressing need to find effective drugs to treat AD (Kuo and Rajesh 2019). Some drugs are currently approved for the management of AD.

Tacrine was the first drug approved for the treatment of AD but was withdrawn due to hepatotoxicity (Ríos *et al*. 2019). Nonetheless, tacrine derivatives have been reported to display promising biological outcomes (Romero and Marco-Contelles 2017, Romero *et al*. 2013). Tacrine increases cerebral blood flow and blocks the release of Beta-amyloid precursor protein, making it a promising drug that can be further modified (Nordberg 1996, Harkins *et al*. 1997, Summers 2022). Memantine is also approved for the treatment of moderate to severe AD (Tariot *et al*. 2004). It is a moderate-affinity uncompetitive *N*-methyl-*D*-aspartate receptor antagonist (Tariot *et al*. 2004). It prevents pathologically high levels of glutamate that are in control of neuronal dysfunction (Danysz and Parsons 2003). Different therapeutics have been developed for the management of AD.

The combination of memantine with a derivative of tacrine, 6-chloro-tacrine displayed a good inhibition effect against the action of acetylcholinesterase and *N*-methyl-*D*-aspartate receptor (Kaniakova *et al*. 2019). 7-methoxytacrine-memantine, a hybrid molecule effectively impeded Aβ peptide amyloid fibrillization, influenced the BACE1 task, and displayed a promising AChE inhibitory effect (Gazova *et al*. 2017). Cinnamic structures linked with either *N,N*-dibenzyl(*N*-methyl)-amine (DBMA) or *N*-benzylpiperidine DBMA displayed

CONTACT Blessing Atim Aderibigbe blessingaderibigbe@gmail.com University of Fort Hare, Chemistry, Alice, 5700 South Africa

antioxidant and neuroprotective properties against mitochondrial oxidative stress and cholinesterases (Danysz and Parsons 2003). Cinnamic acid derivative prepared by fusing N-benzyl pyridinium moiety with different substituted cinnamic acids exhibited potent cholinesterase inhibitory activity with good neuroprotection on PC12 cells. *Ex vivo* investigations in OF1 mice confirmed the compound's capability to traverse the BBB (Lan *et al*. 2017). Cinnamic acid-tryptamine hybrid also displayed a significant *in vitro* inhibitory effect against acetylcholinesterase (AChE) and butyrylcholinesterase (BChE) (Ghafary *et al*. 2020).

Nanotechnology is a promising approach to developing therapeutics for the treatment of AD at all stages of the disorder (Cano *et al*. 2021; Dan and Sharma 2022). Engineered nanoparticles target the brain with high specificity to the brain capillary endothelial cells, display high affinity for amyloid-(A) forms, hinder the generations of amyloid precursor proteins, can be transported throughout the BBB through endocytosis or transcytosis, helps to improve the activity of the multidrug transporters in the blood-brain barrier, displays neuroprotective effects, making it a great and noteworthy platform for the development of therapeutics for early diagnosis and the treatment of AD (Nikalje 2015, Silva-Abreu *et al*. 2018, Lv *et al*. 2020, , Sarathlal *et al*. 2021). The delivery of medications to the brain using nanoparticles has been reported for neurodegenerative disorders, such as Parkinson's Syndrome and AD (Muntimadugu *et al*. 2016, Chen *et al*. 2019, Arisoy *et al*. 2020, ; Zhang *et al*. 2021b).

Polymer-drug conjugate is a nanotherapeutics for drug delivery (Machtakova *et al*. 2022). Currently, there are few reports on polymer-drug conjugates for the treatment of neurological disorders (Heath *et al*. 2016, Sun *et al*. 2017, Aderibigbe *et al*. 2020). The few reports revealed the stability of the conjugates in a physiological environment, non-toxicity, and targeted uptake (Aderibigbe *et al*. 2020, Machtakova *et al*. 2022,). They exhibit special features, such as protecting the loaded drugs from degradation, minimising toxic side effects, and targeted drug transport to the brain, making them promising therapeutics to be investigated for the management of AD (Aderibigbe *et al*. 2020, Machtakova *et al*. 2022). There are currently no reports on polymer-drug conjugates containing tacrine, memantine or cinnamic as anti-AD drugs. Due to the promising features of polymer-drug conjugates, a class of polyamidoamine-based polymer-drug conjugates containing tacrine, memantine and cinnamic acid were synthesised, characterised, and *in vitro* biological study was performed to reveal their potential application for the management of AD.

2. Experimental

2.1. Material and method

The chemicals used were of analytical grade and purchased from Merck Chemical (South Africa) which include propane-1,2-diamine (PDA), *N'N*-methylenebisacrylamide (MBA), *N,N'*-diethyl-1,3-propane diamine (DEP), triethylamine (TEA), dopamine hydrochloride, tacrine, memantine, hydrochloric acid, and cinnamic. Dialysis membranes with a molecular mass cut-off of 12000-14000 were purchased from Merck Chemical (South Africa). Distilled water was used to prepare all the conjugates.

2.2. Procedure for the synthesis of (E)-N-(3-aminopropyl)cinnamide

PDA (500 mg) was dissolved in dried DMF (10 ml). Cinnamic acid (145.09 mg) was added to the reaction mixture followed by the addition of DCC (222.3 mg) and HSU (167.07 mg). The reaction mixture was refluxed at 120 °C for 24 h. The reaction was monitored by TLC (Dichloromethane: Ethyl acetate (7:3)). FTIR results 3302, 2927, 1626, and 1600-1532 cm^{-1}.

2.3. General preparation method of polymer drug conjugate

MBA (0.50 g, 3.24 mmol) was dissolved in 10 ml of warm distilled water. DEP (0.34 g, 0.59 mmol) was added. The resultant solution was flushed with nitrogen gas and stirred continuously at room temperature for over 24 h. Individual drugs were added sequentially and allowed to stir for a period of 24 h after individual drug addiction. 1 ml of TEA was used to maintain a basic medium throughout the reaction. After the addition of the required reagents, the resultant solution was stirred at room temperature for 3 days. The pH was adjusted between 7–8 using concentrated hydrochloric acid and exhaustive dialysis was performed against water followed by freeze-drying to obtain water-soluble solids (Figure 1) (Table 1).

2.4. Characterisation

The polymer-drug conjugates were characterised using known techniques, such as FTIR, ^{1}H NMR, LC-MS, TEM, SEM/EDX, XRD, and particle size analysis followed by

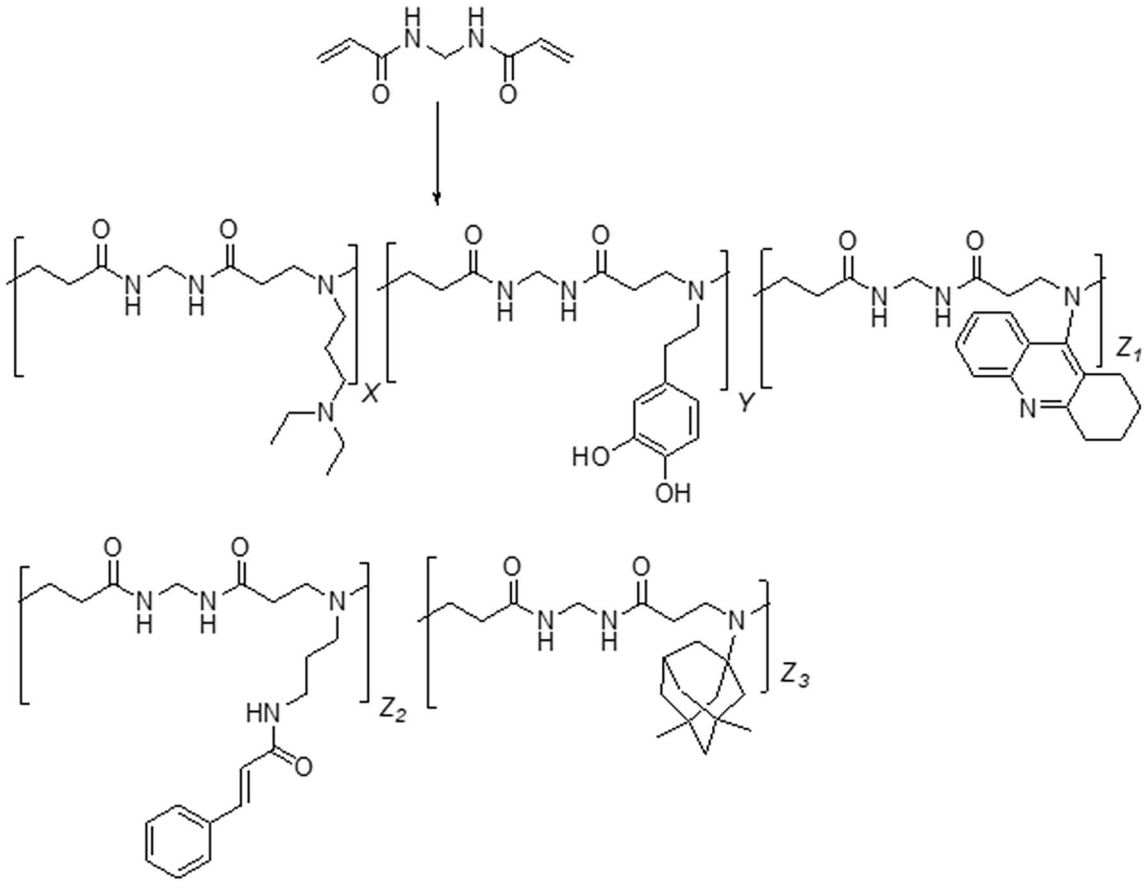

Conjugates	DEP	Y (Dopamine)	Z_1 (Tacrine)	Z_2 ((*E*)-*N*-(3-aminopropyl)cinnamide)	Z_3 (Memantine)
T8	√	√	-	-	√
T9	√	√	√	-	-
T10	√	√	-	√	-
T11	√	√	√	-	√
T12	√	√	√	√	-
T13	√	√	-	√	√

Figure 1. The structures of the synthesised conjugates incorporated with selected drug systems, **T8** conjugate incorporated with memantine, **T9** conjugate incorporated with tacrine**, T10** conjugate incorporated with (E)-N-(3-aminopropyl)cinnamide, **T11** conjugate incorporated with a combination of memantine with tacrine, **T12** conjugate incorporated with a combination of tacrine and *(E)-N*-(3-aminopropyl)cinnamide, and **T13** conjugate incorporated with a combination of memantine and (E)-N-(3-aminopropyl)cinnamide.

in vitro drug release and Anti-acetylcholinesterase (Anti-Alzheimer) studies (*in vitro* and in silico).

2.4.1. Ftir

FTIR analysis was performed on all the conjugates. It was performed in the range of 4000–500 cm^{-1}. It was used to determine the functional groups present in the conjugates and to confirm the successful incorporation of the drugs in the conjugates. It was performed on a Perkin Elmer spectrum 100 FTIR spectrometer.

2.4.2. Nmr

^{1}H NMR spectroscopy was performed using D_2O/Sodium hydroxide on Varian Unity INOVA 300 MHz Nuclear Magnetic Resonance Spectrometer. The NMR samples of all the polymer-drug conjugates were adjusted to pH 10–11 using sodium hydroxide to eliminate protonation.

2.4.3. Sem

The polymer-drug conjugates were sputtered with gold nanoparticles before SEM analysis was performed

Table 1. The composition of prepared polymer-drug conjugates, T8–13 (where **T8** is incorporated with memantine, **T9** is incorporated with tacrine**, T10** is incorporated with (E)-N-*(*3-aminopropyl)cinnamide, **T11** is incorporated with a combination of memantine with tacrine, **T12** is incorporated with a combination of tacrine and *(E)-N-*(3-aminopropyl)cinnamide, and **T13 is** incorporated with a combination of memantine and *(*E)-N-(3-aminopropyl)cinnamide).

Conjugates	MBA (g, mmol)	DEP (g, mmol)	Memantine (g, mmol)	Tacrine (g, mmol)	(*E*)-*N*-(3-aminopropyl) cinnamide	Dopamine (g, mmol)	Colour	Yield (g)
T8	0.50, 3.24	0.34, 2.59	0.06, 0.32	–	–	0.03, 0.16	Dark brown	0.09
T9	0.50, 3.24	0.34, 2.59	–	0.06, 0.32	–	0.03, 0.16	Dark brown	0.14
T10	0.50, 3.24	0.34, 2.59	–	–	0.05, 032	0.03, 0.16	Dark brown	0.08
T11	0.50, 3.24	0.34, 2.59	0.03, 0.16	0.03, 0.16	–	0.03, 0.16	Dark brown	0.15
T12	0.50, 3.24	0.34, 2.59	–	0.03, 0.16	0.025, 0.16	0.03, 0.16	Dark brown	0.08
T13	0.50, 3.24	0.34, 2.59	0.03, 0.16	–	0.025, 0.16		Dark brown	0.17

Propane-1,2-diamine (PDA), *N'N*-methylenebisacrylamide (MBA), *N,N'*-diethyl-1,3-propane diamine (DEP), and triethylamine (TEA). 1 ml of TEA wa used for preparation of the conjugates.

on a JEOL JSM 6390 LV SEM (Japanese Electron Optical Lab.). It was used to evaluate the morphology of the polymer-drug conjugates.

2.4.4. Xrd

X-ray powder diffraction patterns were recorded on a Bruker D8 Discover equipped with a proportional counter, using Cu-Kα radiation ($\lambda = 1.5405$ Å, nickel filter). Data were collected in the range of $2\theta = 10$–100°, scanning at 1.5° min^{-1} with a filter time constant of 0.38 s per step and a slit width of 6.0 mm. The samples were placed on a silicon wafer slide. The X-ray diffraction data were evaluated using the Eva (evaluation curve fitting) software. Baseline correction was performed on each diffraction pattern by subtracting a spline function fitted to the curved background. It was used to confirm the incorporation of the drugs in the prepared conjugates.

2.4.5. Tem and edx

TEM was used to evaluate the morphology of the conjugates. The conjugate samples were dispersed in water and a drop of the solution was placed on the copper gratings. The moist copper gratings were dried on filter paper at room temperature for 15 min before the TEM analysis. TEM analysis was performed on JEM-1200EX, JEOL. The EDX analysis was performed to identify the elemental composition of the polymer-drug conjugates.

2.4.6. LC-Ms

LC-MS analysis was performed on the polymer conjugates to confirm the successful formation of the conjugates and the drug conjugation into the polymer. The analysis was performed on selected conjugates, T8, T9, T11, and T12. A Waters Synapt G2 Quadrupole time-of-flight (QTOF) mass spectrometer (MS) connected to a Waters Acquity ultra-performance liquid chromatograph (UPLC) (Waters, Milford, MA, USA). A Waters BEH C_{18}, 2.1×100 mm, 1.7 µm column was used to facilitate the separation of compounds before data acquisition using a photodiode array detector (PDA), followed by the QTOF MS where data was acquired by scanning from m/z 150 to 1500 m/z in resolution mode as well as in MSE mode. In MSE mode two channels of MS data were acquired, one at low collision energy (4 V) and the second using a collision energy ramp ($40 - 100$ V) to obtain fragmentation data as well. Leucine enkephalin was used as lock mass (reference mass) for accurate mass determination and the instrument was calibrated with sodium formate. An injection volume of 3 µL was used and the mobile phase consisted of 0.1% formic acid (solvent A) and acetonitrile containing 0.1% formic acid as solvent B.

2.4.7. Hydrodynamic properties of the polymer-drug conjugates

Hydrodynamic properties of the conjugates were obtained using a Malvern zeta sizer nano zs (Malvern, United Kingdom). Refractive index: 1.384 and absorption value: 0.001. The analysis was performed on samples labelled T8, T10, T11, T12 and T13 in acetate buffer (pH 5.5) simulating the microenvironment of endosomes of the Alzheimer's disease gene variant. The aqueous buffer samples were all filtered through 0.45 µm syringe filters. The results are given as mean value ± standard deviation (SD) for each parameter measured.

2.4.8. Drug release studies

Buffer solutions at pH 5.5 were prepared and placed in a water bath shaker-BS-06 Lab Companion (set at 37 °C) overnight to equilibrate. Conjugate **T8–T10** (5 mg) was placed in a 10 ml buffer solution in a dialysis membrane and incubated in a water bath set at 37 °C. At 40 min intervals (for the first 10 h), 4 ml of the buffer was removed and replaced with an equivalent amount. The procedure was repeated after 24, 48 and 72 h. The percentage cumulative drug released

was calculated using the equation below:

$$\frac{X}{Y} \text{ X } 100 \quad (1)$$

where X = initial amount of drug released at time t; Y = the total amount of drug loaded in the polymer-drug conjugates. Using the percentage of cumulative release data obtained from Equation (1), different drug release kinetics models were employed, such as Korsmeyer Peppas, Zero Order, and Higuchi (Dash *et al*. 2010).

Korsmeyer peppas

The drug release exponent, n reveals the drug release mechanism of the drug delivery system. Where $n = 0.5$ applies to a Fickian diffusion mechanism, $0.50 < n < 1$ represents non-Fickian transport, $n = 1$ (zero-order), and $n > 1.0$ is a super case II transport. To study the release kinetics, data obtained from the *in vitro* drug release studies were plotted as log cumulative percentage drug release versus log time (Dash *et al*. 2010).

*2.4.9. Anti-acetylcholinesterase (anti-Alzheimer) analysis (*in vitro *and* in silico*)*

The sample inhibitors were dissolved at 100x concentration in an appropriate solvent. Samples T8–T13 were dissolved in water and samples T14–T16 were dissolved in DMF. T14–T16 were further diluted in a ratio of 1:1 in water. In a flat bottom 96-well plate, 10 µl of sample inhibitors at 3 serial dilution concentrations were added into the designated well. 10 µl of diluted acetylcholinesterase was added to each well-containing sample inhibitor compound, inhibitor control [donezepil], and enzyme control [AChE Assay buffer]. The volume of each well was adjusted to 160 µl/well by adding 140 µl of AChE Assay Buffer. After mixing, it was incubated at room temperature for 15 min and protected from light. Absorbance (OD at 412 nm) was measured in kinetic mode for 40 min at room temperature. Time points were chosen and the corresponding values for the absorbance were obtained.

Molecular docking was used to study the in-silico molecular interaction of acetylcholinesterase (protein target) with the samples T8–T13. The crystal structure of the protein target was downloaded from the RSCB protein data bank (PDB), code number 3I6M. The protein preparation module in Schrodinger Maestro (ref) was used to prepare the three-dimensional structure of acetylcholinesterase for virtual screening. The binding site was defined as the region occupied by the co-crystallized ligand using the receptor grid generation module in Schrodinger Maestro. The ligands were also prepared for virtual screening using the ligprep module in the same software. The chemical structure of conjugated drugs was simplified as one drug molecule linked to a five-carbon monomer of the conjugating polymer. Molecular docking simulation was carried out with the Glide module (standard precision docking) and the top five poses were scored. The logP of the samples T8–T13 was also predicted using Data Warrior.

3. Results

Michael addition polymerisation is a flexible synthetic approach useful for generating polymers ranging from linear to hyperbranched polymers (Sun *et al*. 2017). Aqueous Michael's addition polymerisation technique was used to synthesise the polymer-drug conjugates in this study. The conjugates are prepared in water in a one-pot process and are characterised by linear architectures. The reaction involves a nucleophilic addition of a nucleophile to an α, β-unsaturated carbonyl compound. Under mild reaction conditions, the reaction is useful for forming C–C bonds. The advantages of Michael addition reactions are high conversions, the capability to accommodate high functional groups and favourable reaction rates (Aderibigbe *et al*. 2020). The aza Michael polyaddition of prim-monoamines or bis-sec-amines with bis-acrylamides yields a synthetic polymer called linear polyamidoamines (PAAs) (Marcioni *et al*. 2021). PAAs are polymeric carriers with high structural flexibility. They can be engineered to be biodegradable and biocompatible, and are mostly highly water-soluble and hydrophilic. Their capability to hydrolytically degrade in aqueous systems arise from the amide bond on their backbone. Most of them have demonstrated promising antiviral activity, useful as sensor constituents, heparin complexing agents, heavy metal ion complexing agents, transfection promoters and drug delivery systems (Coué and Engbersen 2011, Marcioni *et al*. 2021). Polymer-drug conjugates are nanoscale systems in which a drug molecule is covalently attached to a polymer backbone (Duro-Castano *et al*. 2015).

3.1. Ftir

FTIR analysis was performed to study the functional groups that are present in the polymer-drug conjugate (Figure 2). Conjugate **T8** showed N-H stretching at 3278 cm^{-1}, C=O stretching at 1670 cm^{-1}, and C-N

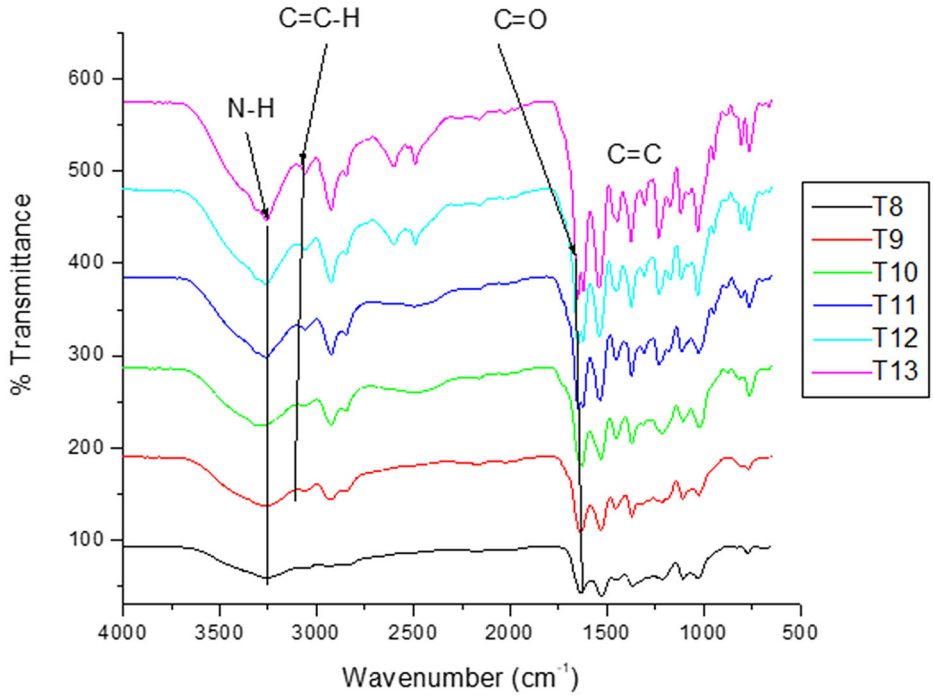

Figure 2. The FTIR spectra of conjugates **T8**, **T9** and **T10** incorporated with memantine, tacrine, and *(E)-N-*(3-aminopropyl)cinnamide, respectively. **T11** incorporated with a combination of memantine with tacrine, **T12** incorporated with a combination of tacrine and *(E)-N-*(3-aminopropyl)cinnamide and **T13** incorporated with a combination of memantine and *(E)-N-(*3-aminopropyl)cinnamide.

stretching at 1023 cm^{-1}. The absorption peaks for conjugate **T9** were visible for N-H stretching at 3373 cm^{-1}, C-H stretching at 2995 cm^{-1}, C-H stretching at 3090 cm^{-1}, C=O stretch at 1661 cm^{-1}, C=C at 1567 cm^{-1}, and C-N stretch at 1023 cm^{-1}. Conjugate **T10** displayed peaks of N-H at 3378 cm^{-1}, C-H at 3072 cm^{-1}, C=C at 1647 cm^{-1}, C=C at 1529 cm^{-1}, and C-N at 1234 cm^{-1} N-H at 3284 cm^{-1}, C-H at 3060 cm^{-1}, C=O at 1647 cm^{-1}, C=C at 1529 cm^{-1}, C-N at 1105 cm^{-1} were visible in conjugate **T11**. Conjugate **T12** showed peaks of N-H at 3272 cm^{-1}, C-H at 3048 cm^{-1}, C=O at 1647 cm^{-1}, C=C at 1541 cm^{-1}, and C-N at 1093 cm^{-1}. Absorption peaks were significant in conjugate **T13** for N-H at 3248 cm^{-1}, C-H at 3013 cm^{-1}, C=O at 1650 cm^{-1}, C=C at 1539 cm^{-1}, and C-N at 1123 cm^{-1}. The characteristic peaks of the amide N-H and C=O confirmed the successful polymerisation reaction. The dominant functional group on the conjugates backbone is the O = CNH-, amide bond that is easily cleaved in the physiological environment. The C=C stretching due to the aromatic rings and the C-N stretching confirmed the successful incorporation of the drugs in the conjugates. Similar absorption peaks were reported for systems loaded with tacrine and memantine (Campos *et al*. 2014, Lokhande *et al*. 2013, Lee and Kim 2015).

3.2. Sem

SEM analysis revealed the surface morphology of the polymer-drug conjugates at different magnifications. The SEM image of conjugate **T8** was a combination of strip-shaped and irregular morphologies (Mahmoudi *et al*. 2021). In conjugate **T9**, a rough surface with spherical and porous surface morphologies was significantć. Conjugates **T10** and **T11** showed a rough surface and porous morphology which was uniformly distributed (Li *et al*. 2016). Conjugate **T12** showed irregular, porous and rough surfaces. The rough surface and strip-shaped morphology were significant for conjugate **T13**. The porous structure of the conjugates indicates their capability to accommodate drugs. The rough surface is an important feature that supports cellular adhesion (Campos *et al*. 2014, Martinez *et al*. 2020).

3.3. Nmr

^{1}H NMR analysis was performed to confirm the structure of polymer-drug conjugates. The ^{1}H NMR signals for the polymer-drug conjugates are shown in Table 2. ^{1}H NMR signals for the conjugates were significant for $N(CH_2\mathbf{CH_3})_2$ protons on the solubilising unit, (DEP) at the range of 0.9-0.93 ppm. The polymer backbone signals for the conjugates were noted for $N\mathbf{CH_2}$ at the shift

Table 2. A summary of important proton signals visible on the ^{1}HNMR spectra for the conjugates, T8–13.

Conjugates	Assignments	Shift range (ppm)	Protons expected	Protons found
T8	(a). CH_3	0.93	51	51
	(b). NCH_2	2.33–2.71	79	80
	(c). $CONHCH_2CONH$	4.54 – 4.44	20	20
	(d).$NHCH_2CH_2CH_2N$,	1.54	9	14
	(e). CH_2CONH, CH_2CNH, CCH_2	2.69–2.68	35	40
T9	(a). $N(CH_2CH_3)_2$	0.90	42	42
	(b). $CONHCH_2CONH$	4.47	20	15
	(c). CH_2CH_2	1.83	14	7
	(d).CH = CH	8.37–6.15	5	4
	(e). CH_2CONH	2.68–2.70	40	42
	(f). NCH_2	2.11–2.70	76	77
T10	(a). $N(CH_2CH_3)_2$,	2.41–2.40	82	77
	(c). $CONHCH_2CONH$	4.44	20	20
	(d). $NHCH_2CH_2CH_2N$	1.18	14	17
	(e).CH = CH	8.33	6	8
	(f). CH_2CONH	2.27	40	34
T11	(a). CH_3	1.14	42	42
	(b). NCH_2	2.60–2.31	78	76
	(c). $CONHCH_2CONH$	4.47	20	16
	(d). CH_2CNH, CCH_2 and CH_2CH_2	1.52–1.17	14	16
	(e).CH = CH	8.36–6.15	3	2
	(f). CH_2CONH	2.70–2.68	40	33
T12	(a). $N(CH_2CH_3)_2$	0.86	42	42
	(b). NCH_2	2.44–2.41	80	77
	(c). $CONHCH_2CONH$	4.56–4.53	20	12
	(d). CH_2CH_2	1.53	16	16
	(e).CH = CH	8.37–6.15	8	2
	(f). CH_2CONH	2.70–2.68	40	35
T13	(a). CH_3	0.90	48	48
	(b). NCH_2	2.31–2.46	80	71
	(c). $CONHCH_2CONH$	4.56–4.57	20	22
	(d). CH_2CNH, CCH_2	1.53–1.52	16	12
	(e).CH = CH	8.36–6.15	8	4
	(f). CH_2CONH	2.70–2.68	40	42

Conjugate **T8** incorporated with memantine, **T9** incorporated with tacrine, **T10** incorporated with (E)-N-(3-aminopropyl)cinnamide, **T11** incorporated a combination of memantine with tacrine, **T12** incorporated with a combination of tacrine and *(E)-N*-(3-aminopropyl)cinnamide, and **T13** incorporated with a combination of memantine and (E)-N-(3-aminopropyl)cinnamide.

range of 2.33-2.71 ppm, $CONH\mathbf{CH_2}CONH$ at 4.54 – 4.44 ppm, $NHCH_2\mathbf{CH_2}CH_2N$ at 1.53 ppm and $\mathbf{CH_2}CONH$ at 2.69-2.68. The protons due to memantine were visible for $\mathbf{CH_2}CH_2CH_3$ at the shift range of 0.86 ppm (Lokhande *et al*. 2013). The aromatic protons of tacrine (Sharma *et al*. 2020), dopamine, and **(***E*)-*N*-(3-aminopropyl)cinnamide were visible in the range of 8.37-6.15 ppm for the conjugates. The protons of the aromatic ring on the cinnamic derivative confirmed its successful conjugation in the prepared conjugates and similar findings were reported for nanocarriers loaded with cinnamic derivatives (Lee and Kim 2015, Zhao *et al*. 2019). The mass percentage incorporation of the drugs in the conjugates based on the ^{1}HNMR spectra was found to be 3.3 w/w % of memantine in T8, T9 (6.0 w/w % Tacrine), T10 (4.2% Cinnamic acid), T11 (3.3 w/w % Memantine and 3.5 w/w % Tacrine), T12 (4.8 w/w% Memantine and 1.3% Cinnamic acid), T13 (2.5 w/w % Tacrine and 2.5 w/w % Cinnamic acid). The ^{1}HNMR and percentage incorporation of the drugs confirmed the successful incorporation of the drugs in the PDC.

3.4. Xrd

The XRD thermographs of the selected conjugates (T9-T12) are shown in Figure 3. The thermographs revealed broad peaks indicating an amorphous nature of the conjugates. The absence of significant crystalline peaks of the drugs for conjugates **T9** and **T11** confirmed the absence of free drugs and the successful incorporation of the drugs into the polymer. In conjugate **T10** containing **(***E*)-*N*-(3-aminopropyl) cinnamide only and conjugate **T12** containing a combination of **(***E*)-*N*-(3-aminopropyl)-cinnamide and tacrine, sharp peaks were visible but are not attributed to free drugs. The sharp peaks are attributed to the crystalline nature of (*E*)-*N*-(3-aminopropyl)cinnamide incorporated in the conjugates. A similar finding was reported by (Sadeghi *et al*. 2020). The decrease in the crystalline nature of (*E*)-*N*-(3-aminopropyl)cinnamide suggests its successful incorporation into the polymer backbone. The amorphous nature of the conjugates also indicates a higher drug-loading capacity of polymer-drug conjugates (Singh *et al*. 2015).

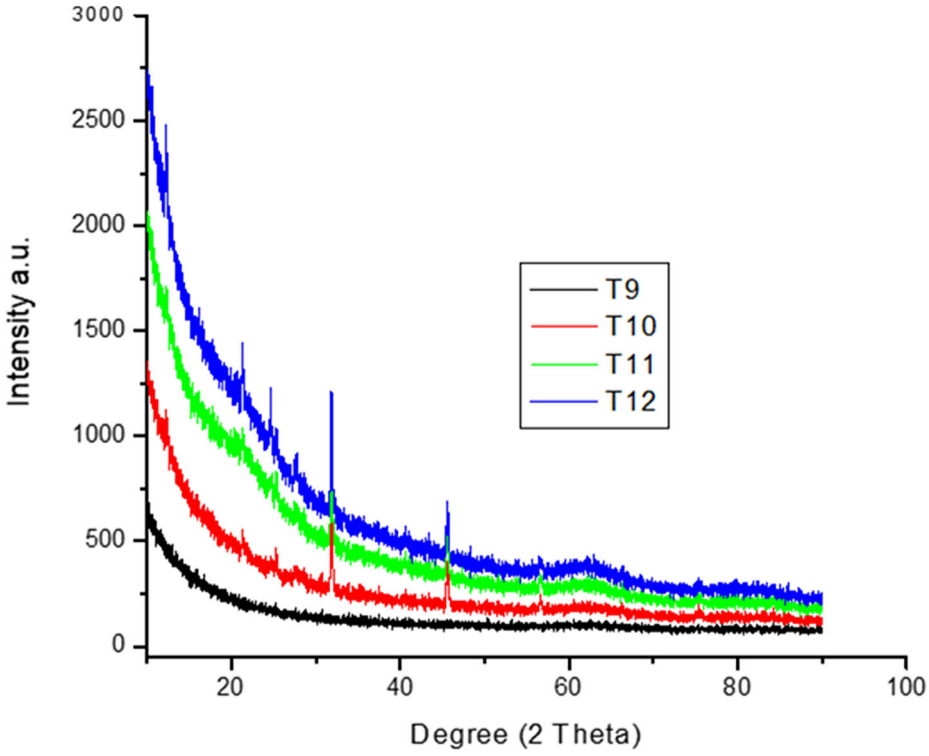

Figure 3. The XRD thermographs of conjugates revealin the amorphous nature of the conjugates in which **T9 is** incorporated with tacrine, **T10** is incorporated with (E)-N-*(*3-aminopropyl)cinnamide, **T11** is incorporated with a combination of memantine with tacrine, and **T12** is incorporated with a combination of tacrine and *(E)-N-*(3-aminopropyl)cinnamide.

3.5. Tem and EDX

TEM analysis further revealed the morphology and particle size of the polymer-drug conjugates (Figure 4). TEM image of conjugate **T8** showed spherical-shaped morphology. Spherically-shaped nanocarriers have been reported to exhibit high accumulation in the brain, making them useful for brain targeting (Da Silva-Candal *et al*. 2019). Conjugate **T9** displayed particle size in the range of 7.86 nm-22.68 nm. **T12** and **T13** conjugates loaded with (*E*)-*N*-(3-aminopropyl)cinnamide also displayed spherical morphology. TEM results of nanoparticle sizes in the same range were reported by Youssif *et al.* and found to be appropriate for effective brain targeting (Konda *et al*. 2012, Youssif *et al*. 2019,).

The elemental composition of the polymer-drug conjugates was determined using EDX (Table 3). The percentage of carbon was in the range of 43.32–61.41% and nitrogen was in the range of 12.74–20.03 w/w %. The percentage composition of oxygen was in the range of 10.09–26.96 w/w%. Conjugates containing **(***E*)-*N*-(3-aminopropyl)cinnamide displayed the highest percentage of carbon due to the presence of the long carbon chain which further confirmed the successful incorporation of the drugs in the conjugates.

3.6. LC-Ms

LC-MS analysis was performed on the polymer-drug conjugates to verify the formation of the conjugates (**T8**–**T12**) and the drug conjugation into the polymer. The fragment peaks for conjugate **T8** were visible at m/z = 178, 181 and 182 which are attributed to the fragmentation of memantine. Almeida *et al* recorded the similar fragment peaks for memantine (Konda et al. 2012, Leis and Windischhofer 2012, Badawi *et al*. 2022). In conjugate **T9,** fragment ions peaks were visible at m/z = 199 for tacrine. Tacrine fragment peaks were also reported by (Rajasekhar et al. 2018) Conjugate **T11** showed drug fragment peaks at m/z = 180 and 199, peaks for the incorporated drugs. Conjugate **T12** exhibited fragment peaks at m/z = 199 and 203. The fragments found in conjugates (**T8**, **T9**, **T11** and **T12**) confirmed the successful incorporation of drugs into the polymer.

3.7. Hydrodynamic properties of polymer-drug conjugates

The PDI of the polymer-drug conjugates was in the range of 0.309 ± 0.025 to 1.000 (Table 3). The conjugates loaded with a single drug together with the targeting moiety displayed higher PDI values of 1.00 and

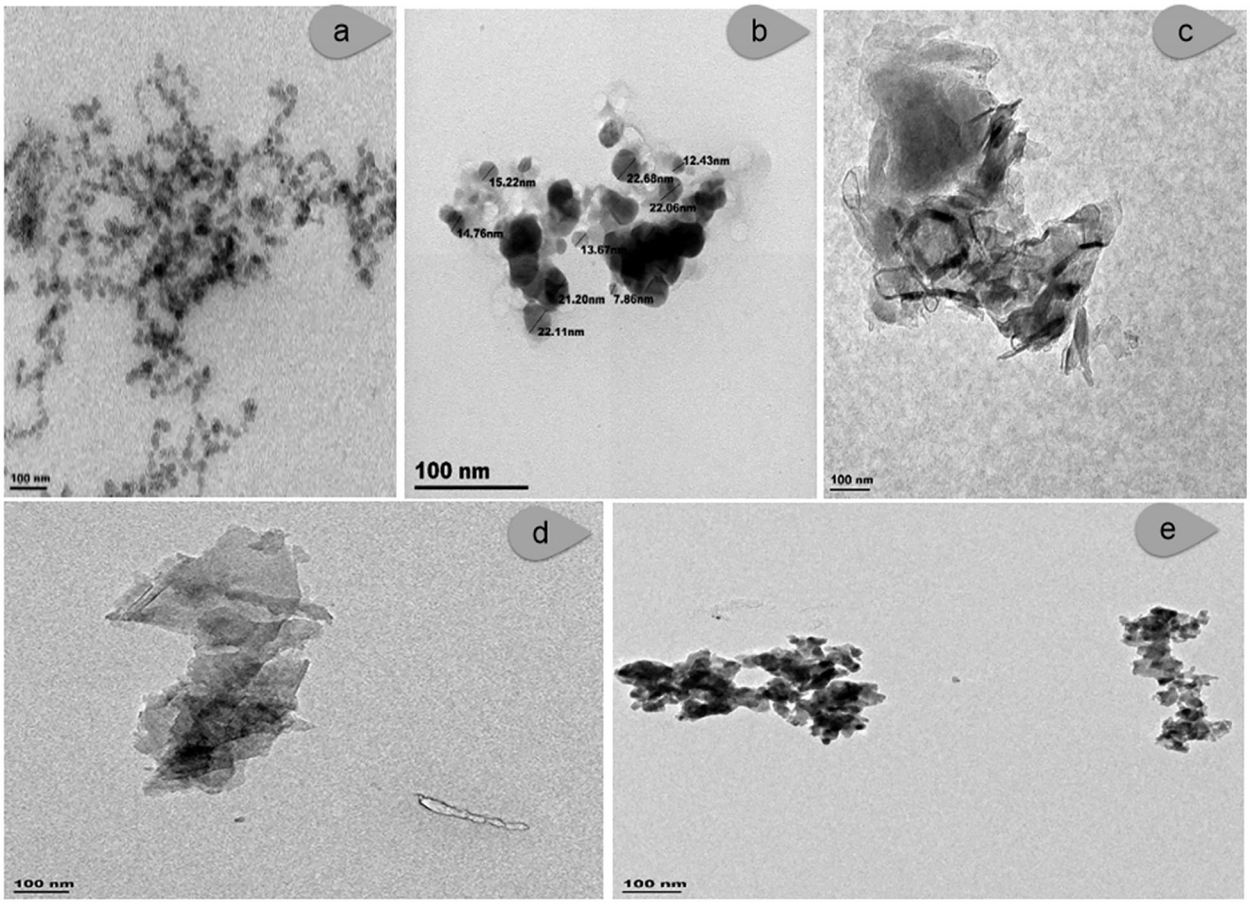

Figure 4. The TEM images of the conjugates revealing the morphology of the polymer-drug conjugates where**: T8** incorporated with memantine (b) **T9** incorporated with tacrine (c) **T11** incorporated with a combination of memantine with tacrine (d) **T12** incorporated with the combination of tacrine and *(E)-N*-(3-aminopropyl)cinnamide (e) **T13** incorporated with a combination of memantine and *(*E)-N-(3-aminopropyl)cinnamide.

Table 3. Hydrodynamic studies of polymer-drug conjugates, T8–13 showing the particle size (d.nm)±SD, PDI ± SD, and the Surface charge (mV) ± SD (where $n = 3$) and elemental composition of the conjugates, T8-13 obtained from SEM-EDX.

Samples	Mean Particle Diameter (d.nm) ± SD	PDI ± SD	Surface charge (mV) ± SD	Elemental composition C (w/w%), N (w/w%), O (w/w%)
T8	3075.0 ± 831.30	1.000	6.32 ± 2.46	51.59, 16.22, 26.96
T9	–	–	–	43.32, 17.31, 12.27
T10	243.9 ± 32.60	0.515 ± 0.147	5.45 ± 1.36	58.84, 13.74, 10.09
T11	271.0 ± 6.58	0.309 ± 0.025	1.05 ± 0.103	46.92, 20.03, 15.23
T12	393.4 ± 14.26	0.346 ± 0.024	9.64 ± 0.452	61.41, 12.74, 10.99
T13	499.4 ± 74.13	0.497 ± 0.028	3.71 ± 1.38	61.41, 12.74, 15.20

Conjugate **T8** incorporated with memantine, **T9** incorporated with tacrine**, T10** incorporated with (E)-N-(3-aminopropyl)cinnamide, **T11** incorporated with a combination of memantine with tacrine, **T12** incorporated with a combination of tacrine and *(E)-N*-(3-aminopropyl)cinnamide, and **T13** incorporated with a combination of memantine and *(*E)-N-(3-aminopropyl)cinnamide.

0.515 ± 0.147, respectively for **T8** and **T10** revealing a high polydispersity and a highly broad particle size distribution. The PDI values of **T11–T13** were less than 0.5, revealing a narrow size distribution (Ghogari and Jain 2020, Monge-Fuentes *et al*. 2021). The zeta potential is a measure of an index for particle stability and cell membrane interaction. The conjugates displayed a neutral charge surface in the range of 1.05 ± 0.103-9.64 ± 0.452.

The surface charge of the polymeric nanoparticles has a crucial influence on BBB penetration. The BBB endothelial cells are characterised by a higher density of negative charges resulting from the presence of proteoglycans. Positively charged nanoparticles can cross the BBB via adsorptive-mediated transcytosis (Chen and Liu 2012, Hettiarachchi *et al*. 2019,). However, positively charged nanoparticles have been reported to induce higher toxicity when compared to

anionic and neutral nanoparticles. Neutral nanoparticles do not have an impact on the BBB integrity while anionic and cationic nanoparticles have been reported to disrupt the BBB, inducing toxic effects on brain microvasculature endothelium (Ribovski *et al*. 2021). Neutrally charged nanoparticles display lower protein adsorption, resulting in an extended circulation time (Li and Sabliov 2013). When administered intravenously, they display a longer circulation time (Lombardo *et al*. 2020). Neutrally charged nanoparticles have been reported to accumulate more in an injured brain than positively charged nanoparticles with a reduced accumulation in off-target organs such as the heart, lung, and kidneys, suggesting that a reduced cellular association results in reduced restricted movement (Kumar and Nadu 2018).

The particle sizes of the conjugates were in the range of 243.9 ± 32.60-3075 ± 831.3 nm. The particle sizes of the conjugates, (**T10–T12**) were less than 400 nm. Nanoparticles in a size range of 12-340 nm have been established to cross the BBB (Lombardo *et al*. 2020). Generally, the drug-loaded nanoparticles are administered orally or intravenously. In oral administration, polymeric nanoparticles with particle size less than 500 nm are easily taken up by the lymphatic system thereby improving drug bioavailability. When administered intravenously, particle sizes less than 200 nm exhibit a low rate of clearance with an extended circulation time (Kulkarni and Feng 2013).

3.8. In vitro *drug release studies*

In vitro drug release studies were performed at pH 5.5 for conjugates T8–T10. In conjugate T8, the drug release was found to be sustained for 72 h. The sustained release profile is useful for overcoming drug toxicity (Ghogari and Jain 2020). Sustained release of tacrine from loaded poly (lactide-co-glycolide) nanoparticles has been reported (Kumar and Nadu 2018, Singh *et al*. 2019). Nanoparticles allow sustained drug release patterns within the bloodstream, allowing a higher drug concentration to cross the BBB (Zeeshan *et al*. 2019). The % drug release for conjugate **T8** was 36%, conjugate **T9** (31%) and **T10** (20%). The drug release followed a zero-order drug release profile revealing that the drugs are released at a constant rate, prolonging the therapeutic impact as well as avoiding side effects of the drugs (Li *et al*. 2021). The diffusion exponent of memantine, tacrine and cinnamic acid were 1.003, 1.062 and 1.0003 at pH 5.4 with R^2 values of 1, 0.9943 and 1, respectively. The R^2 value in the range of 0.9943 − 1 indicates a good correlation (Wu *et al*. 2019). The conjugates also obeyed the Korsmeyer-Peppas drug release model. A high drug entrapment of NPs with a sustained drug release profile is a promising system for effective brain targeting in diseases like AD (Singh *et al*. 2019).

Table 4. *In vitro* evaluation of the conjugates, T9–13 and the controls against the Acetylcholinesterase (AChE) enzyme ($n = 3$).

Conjugates	Concentrations (μM) at 50% relative inhibition
T8	20.7 ± 4.65
T9	16.5 ± 2.72
T10	12.8 ± 3.54
T11	44.4 ± 10.05
T12	19.4 ± 3.17
T13	20.1 ± 4.47
Controls	
Memantine	3.7 ± 1.14
Tacrine	1698.7 ± 64.54
(E)-N-(3-aminopropyl)cinnamide	18.6 ± 4.15

Conjugate **T8** incorporated with memantine, **T9** incorporated with tacrine, **T10** incorporated with (E)-N-(3-aminopropyl)cinnamide, **T11** incorporated a combination of memantine with tacrine, **T12** incorporated with a combination of tacrine and *(E)-N*-(3-aminopropyl)cinnamide, and **T13** incorporated with a combination of memantine and *(E)*-N-(3-aminopropyl)cinnamide.

3.9. In vitro *anti-Alzheimer analysis*

The polymer-drug conjugates, (**T8–T13**) and the controls were evaluated against the human recombinant Acetylcholinesterase (AChE) enzyme (Table 4). Acetylcholinesterase (AChE) persists as a strong viable target for the symptomatic enhancement in AD because the cholinergic deficit is consistence and an early finding in AD (Mehta *et al*. 2012). A common feature of AD is the presence of acetylcholinesterase (AChE) which is associated with β-amyloid plaques and neurofibrillary tangles. The inhibition of AChE is useful in maintaining the normal neurotransmission mediated by acetylcholine in a healthy brain and it is also useful in preventing the occurrence or slowing down the progression of AD (Arya *et al*. 2021). The change in AChE function leads to a loss of nervous system functioning which is common in neurological disorders. Inhibiting AChE is reported to result in clinical success in the treatment of AD (Jiang *et al*. 2018). The IC_{50} values of the conjugates (**T8–T13**) were found to be in the range of 13–44.4 μM when compared to the controls which were 3.7, 1698.8 and 18.6 μM. **T8**, **T11**, and **T13** did not display a potent inhibitory effect when compared to free memantine. However, the conjugates displayed a potent inhibitory effect when compared to tacrine and (*E*)-*N*-(3-aminopropyl)cinnamide. **T10** incorporated with (*E*)-*N*-(3-aminopropyl)cinnamide displayed a more potent inhibitory effect than the free (*E*)-*N*-(3-

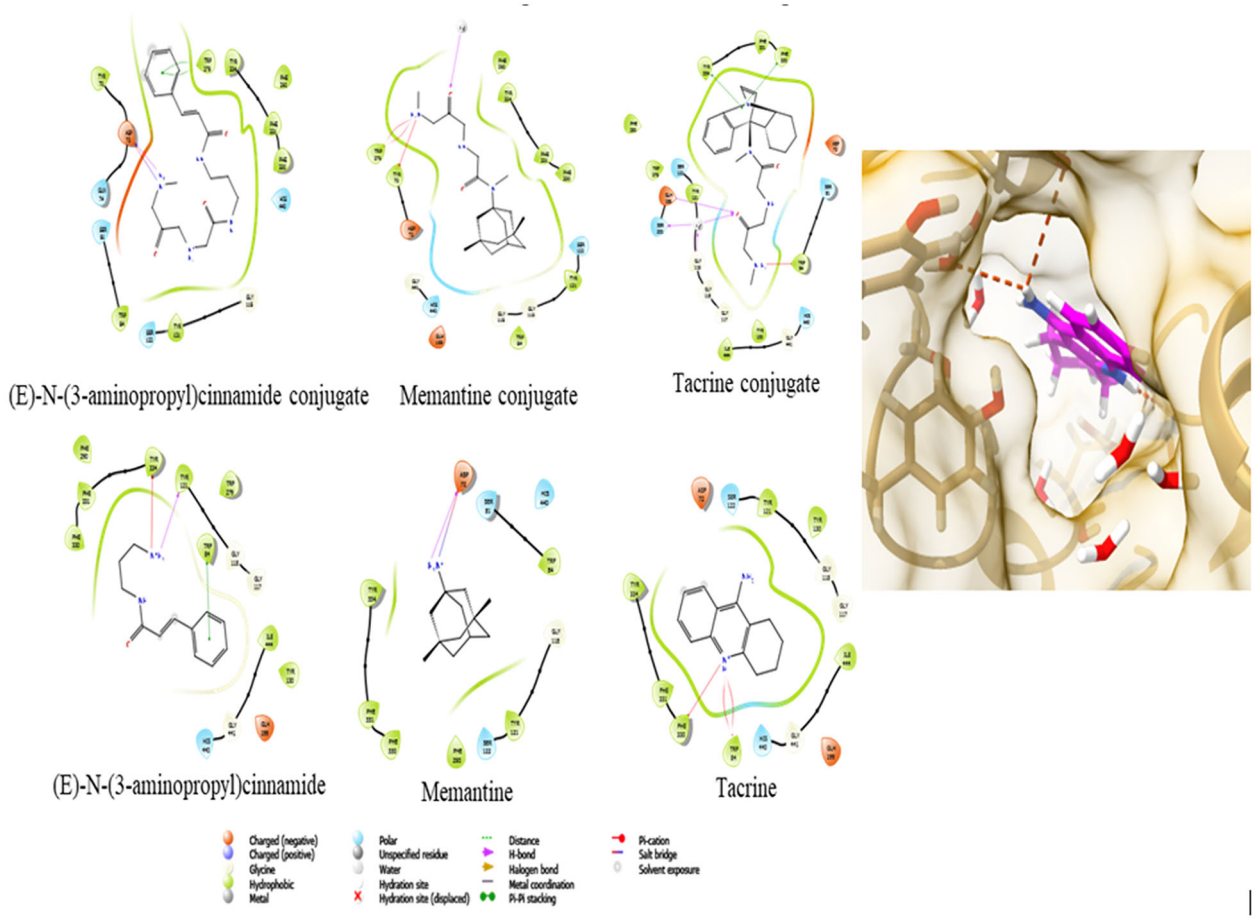

Figure 5. 2 D images of the docked conformations of the conjugates, **T8–10** Panel (right): The deep gorge of the binding pocket of acetylcholinesterase with memantine bound to it. Panel (left): The visualisation of the protein-ligand interaction between the samples T8–T10, the free drugs, (E)-N-(3-aminopropyl)cinnamide, tacrine, and memantine and the binding site of acetylcholinesterase.

aminopropyl)cinnamide. The combination of the two drugs in the polymer did not enhance the inhibitory effect. The conjugates displayed a promising inhibitory effect. Conjugates **T12** and **T13** displayed comparable inhibition effects as (*E*)-*N*-(3-aminopropyl)cinnamide. Tacrine has been reported to be more potent in inhibiting BuchE than AChE (Marucci *et al*. 2021). However, it is no longer in use due to its hepatotoxicity (Marucci *et al*. 2021).′ *N*-alkyl-7-methoxytacrine hydrochloride is one of the tacrine analogues that has been proven to have marked inhibitory activity (Vecchio *et al*. 2021). A good inhibitory effect against AChE has been noted for a novel cinnamic derivative (Lan *et al*. 2017) and 2-Chlorophenyl (2E)-3–(3,4,5-trimethoxyphenyl)prop-2-enoate (Kos *et al*. 2021). Comparing the single drug-loaded conjugates, (**T8–T10**) with the dual drug-loaded conjugates, (**T11–13**), the combination therapy did not induce a better inhibition effect than the single therapy. It has been reported that combination therapy can be more effective in enhancing neuropsychiatric behaviours because of the synergistic effect (Li *et al*. 2015). The findings from this study suggest that PDCs have a promising inhibitory effect and are useful for treating Alzheimer's disease.

An *in silico* study using molecular docking gave insight into the observed anti-acetylcholinesterase activities. The results (Figure 5) showed that Tacrine had a slightly stronger binding affinity (lower binding energy) to the acetylcholinesterase binding site than the Tacrine conjugate. This tends to align with the observed in-vitro activity which showed that the unconjugated tacrine had better anti-acetylcholinesterase activity than the conjugated Tacrine. Protein-ligand interaction visualisation showed that the conjugation might have reoriented the molecule such that the tacrine portion no longer has access to the acyl-binding pocket within the gorge of the active site of the acetylcholinesterase. Unconjugated memantine showed a better binding affinity for the acetylcholinesterase than the conjugated memantine which correlated with the observed *in vitro*. Better access to the acyl-binding pocket within the gorge of the active site

of the acetylcholinesterase might also be a reason for this observation. However, the conjugated (***E*)-***N*-(3-aminopropyl)cinnamide seems to show a better binding affinity for the acetylcholinesterase than the unconjugated compound. Protein-ligand interaction visualisation showed that the conjugated (***E*)-***N*-(3-aminopropyl)cinnamide had more hydrogen bond interactions and available surface for hydrophobic interactions than the unconjugated (***E*)-***N*-(3-aminopropyl)cinnamide. Overall, the conjugation seems to improve the anti-acetylcholinesterase activity of (***E*)-***N*-(3-aminopropyl)cinnamide but might not have a positive effect on the activities of tacrine and memantine.

Predicted logP for the samples showed that the conjugation led to increased predicted logP values (increased hydrophobicity) for tacrine and (***E*)-***N*-(3-aminopropyl)cinnamide. However, the conjugation of memantine led to a decreased logP value. Although log P has been recognised as a key factor that contributes to the bioactivity of a molecule, increasing hydrophobicity is associated with increased bioactivity however, this trend was not observed in the samples in this study (Martin 2018).

4. Conclusion

The ^{1}HNMR and FTIR spectra of the conjugates showed the expected signals and peaks confirming the successful preparation of the polymer-drug conjugates. The absence of free drugs and the amorphous nature of the conjugates displayed by the XRD thermograph confirmed the successful incorporation of the drugs in the conjugates. The positive surface charge, sustained drug release profile, and particle sizes of the conjugates are useful features for brain targeting. The conjugates' good water solubility further revealed the advantage of polymer-drug conjugates when compared to most conventional drugs that suffer from poor water solubility. Their good inhibitory effects against AChE reveal their promising application as therapeutics for the treatment of AD. However, further research is needed to fully understand the mode of action of these conjugates.

Disclosure statement

No potential conflict of interest was reported by the author(s).

Funding

The financial assistance of the Govan Mbeki Research and Development Council, University of Fort Hare, Medical Research Council, and National Research Foundation, South Africa, towards this research are hereby acknowledged. The views and opinions expressed in this manuscript are those of the authors and not of MRC or NRF. This work was supported by South African National Research Foundation; South African Medical Research Council.

References

Aderibigbe, B.A., *et al.*, 2020. Polyamidoamine-drug conjugates containing metal-based anticancer compounds. *Journal of inorganic and organometallic polymers and materials*, 30 (5), 1503–1518.

Arisoy, S., *et al.*, 2020. In vitro and in vivo evaluation of levodopa-loaded nanoparticles for nose-to-brain delivery. *Pharmaceutical development and technology*, 25 (6), 735–747. Taylor & Francis,

Arya, A., *et al.*, 2021. Acetylcholinesterase inhibitory potential of various sesquiterpene analogues for Alzheimer's disease therapy. *Biomolecules*, 11 (3), 350.

Badawi, N.M., *et al.*, 2022. Investigating the impact of optimized trans -cinnamic acid-loaded plga nanoparticles on epithelial to mesenchymal transition in breast cancer. *International journal of nanoscience*, 17, 733–750.

Breijyeh, Z., and Karaman, R., 2020. Comprehensive review on Alzheimer's disease. *Molecules*, 25 (24), 5789.

Campos, V., *et al.*, 2014. Characterization of neutrophil adhesion to different titanium surfaces. *Bulletin of materials science*, 37 (1), 157–166.

Cano, A., *et al.*, 2021. Nanomedicine-based technologies and novel biomarkers for the diagnosis and treatment of Alzheimer's disease : from current to future challenges. *Journal of nanobiotechnology*, 19 (1), 1–30.

Chen, T., *et al.*, 2019. Nanoparticles mediating the sustained puerarin release facilitate improved brain delivery to treat parkinson's disease. *ACS applied materials & interfaces*, 11 (48), 45276–45289.

Chen, Y., and Liu, L., 2012. Modern methods for delivery of drugs across the blood–brain barrier. *Advanced drug delivery reviews*, 64 (7), 640–665.

Dan, S., and Sharma, D., 2022. Therapeutic and diagnostic applications of nanocomposites in the treatment Alzheimer's. *Disease studies*, 12 (1), 940–960.

Danysz, W., and Parsons, C.G., 2003. The NMDA receptor antagonist memantine as a symptomatological and neuroprotective treatment for Alzheimer's disease: preclinical evidence. *International journal of geriatric psychiatry*, 18 (Suppl 1), S23–S32.

Dash, S., *et al.*, 2010. Kinetic modeling on drug release from controlled drug delivery systems. *Acta poloniae pharmaceutica*, 67 (3), 217–223.

Da Silva-Candal, A., *et al.*, 2019. Shape effect in active targeting of nanoparticles to inflamed cerebral endothelium under static and flow conditions. *Journal of controlled release: official journal of the controlled release society*, 309, 94–105.

Duro-Castano, A., Movellan, J., and Vicent, M.J., 2015. Smart branched polymer-drug conjugates as nano-sized drug delivery systems. *Biomaterials science*, 3 (10), 1321–1334.

Fan, L., *et al.*, 2019. New insights into the pathogenesis of Alzheimer's disease. *Frontiers in neurology*, 10 (1312), 1312–1312.

Coué, G., and Engbersen, J.F., 2011. Functionalized linear poly (amidoamine)s are efficient vectors for intracellular protein delivery. *Journal of controlled release*, 152 (1), 90–98.

Gazova, Z., *et al.*, 2017. Multi-target-directed therapeutic potential of 7-methoxytacrine-adamantylamine heterodimers in the Alzheimer's disease treatment. *Biochimica et biophysica acta. Molecular basis of disease*, 1863 (2), 607–619.

Ghafary, S., *et al.*, 2020. Design, synthesis, and evaluation of novel cinnamic acid-tryptamine hybrid for inhibition of acetylcholinesterase and butyrylcholinesterase. *Daru : journal of faculty of pharmacy, Tehran University of medical sciences*, 28 (2), 463–477.

Ghogari, I.S., and Jain, P.S., 2020. Original article development of orally disintegrating tablets Of memantine hydrochloride – A remedy for Alzheimer's disease. *International journal of applied pharmaceutics*, 12 (1), 147–152.

Haque, R.U., and Levey, A.I., 2019. Alzheimer's disease : A clinical perspective and future nonhuman primate research opportunities. *Proceedings of the national academy of sciences of the united states of america*, 116 (52), 26224–26229.

Harkins, S.W., *et al.*, 1997. Tacrine treatment in Alzheimer's disease enhances cerebral blood flow and mental status and decreases caregiver suffering. *Annals of the New York academy of sciences*, 826 (1), 472–474.

Heath, F., *et al.*, 2016. A novel PEG-haloperidol conjugate with a non-degradable linker shows the feasibility of using polymer-drug conjugates in a non-prodrug fashion. *Polymer chemistry*, 7 (47), 7204–7210.

Hettiarachchi, S.D., *et al.*, 2019. Nanoparticle-mediated approaches for Alzheimer's disease pathogenesis, diagnosis, and therapeutics. *Journal of controlled release : official journal of the controlled release society*, 314, 125–140.

Jiang, X.Y., *et al.*, 2018. Dual GSK-3β/AChE inhibitors as a new strategy for multitargeting anti-Alzheimer's disease drug discovery. *ACS medicinal chemistry letters*, 9 (3), 171–176.

Kaniakova, M., *et al.*, 2019. Combination of memantine and 6-chlorotacrine as novel multi-target compound against Alzheimer's disease. *Current Alzheimer research*, 16 (9), 821–833.

Konda, R.K., *et al.*, 2012. Bioanalytical method development and validation of memantine in human plasma by high performance liquid chromatography with tandem mass spectrometry : application to bioequivalence study. *Journal of analytical methods in chemistry*, 2012, 101248–101249.

Kos, J., *et al.*, 2021. Trimethoxycinnamates and their cholinesterase inhibitory activity. *Applied sciences*, 11 (10), 4691.

Kulkarni, S.A., and Feng, S.S., 2013. Effects of particle size and surface modification on cellular uptake and biodistribution of polymeric nanoparticles for drug delivery. *Pharmaceutical research*, 30 (10), 2512–2522.

Kumar, S.S., and Nadu, T., 2018. Formulation, characterization and determination of anti-Alzheimer activity of tacrine loaded poly (lactide-co-glycolide) nanoparticles. *IJPSR*, 9 (12), 5111–5120.

Kuo, Y.C., and Rajesh, R., 2019. Challenges in the treatment of Alzheimer's disease: recent progress and treatment strategies of pharmaceuticals targeting notable pathological factors. *Expert review of neurotherapeutics*, 19 (7), 623–652.

Lan, J.S., *et al.*, 2017. Design, synthesis and evaluation of novel cinnamic acid derivatives bearing N-benzyl pyridinium moiety as multifunctional cholinesterase inhibitors for Alzheimer's disease. *Journal of enzyme inhibition and medicinal chemistry*, 32 (1), 776–788.

Lee, J.H., and Kim, J.C., 2015. UV-absorbing and emulsifying property of cinnamic acid-conjugated gelatin. *Journal of dispersion science and technology*, 36 (7), 1000–1008.

Leis, H.J., and Windischhofer, W., 2012. Determination of memantine in human plasma by GC using negative ion chemical ionization MS detection after derivatization with a new reagent. *Microchimica acta*, 178 (3–4), 309–314.

Li, J., and Sabliov, C., 2013. PLA/PLGA nanoparticles for delivery of drugs across the blood–brain barrier. *Nanotechnology reviews*, 2 (3), 241–257.

Li, S.M., Mo, M.S., and Xu, P.Y., 2015. Progress in mechanisms of acetylcholinesterase inhibitors and memantine for the treatment of Alzheimer's disease. *Neuroimmunology and neuroinflammation*, 2 (4), 274–280.

Li, W., *et al.*, 2016. Evaluation of antioxidant ability in vitro and bioavailability of trans-cinnamic acid nanoparticle by liquid antisolvent precipitate. *Journal of nanomaterials*, 2016, 1–11.

Li, X., Li, Q., and Zhao, C., 2021. Zero-order controlled release of water-soluble drugs using a marker pen platform. *ACS omega*, 6 (21), 13774–13778.

Lombardo, S.M., *et al.*, 2020. Key for crossing the BBB with nanoparticles: the rational design. *Beilstein journal of nanotechnology*, 11 (866), 866–883.

Lv, L., *et al.*, 2020. Brain-targeted co-delivery of β-amyloid converting enzyme 1 shRNA and epigallocatechin-3-gallate by multifunctional nanocarriers for Alzheimer's disease treatment. *IUBMB life*, 72 (8), 1819–1829.

Mahmoudi, M., *et al.*, 2021. Preparation and characterization of memantine-loaded polycaprolactone nanocapsules for Alzheimer's disease. *Journal of porous materials*, 28 (1), 205–212.

Marcioni, M., *et al.*, 2021. Semi-crystalline hydrophobic polyamidoamines: a new family of technological materials? *Polymers*, 13 (7), 1018.

Martin, Y.C., 2018. How medicinal chemists learned about log P. *Journal of computer-aided molecular design*, 32 (8), 809–819.

Martinez, M.A.F., *et al.*, 2020. Surface roughness of titanium disks influences the adhesion, proliferation and differentiation of osteogenic properties derived from human. *International journal of implant dentistry*, 6 (1), 1–11.

Marucci, G., *et al.*, 2021. Neuropharmacology efficacy of acetylcholinesterase inhibitors in Alzheimer's disease. *Neuropharmacology*, 190, 108352(1–15).

Mehta, M., *et al.*, 2012. New acetylcholinesterase inhibitors for Alzheimer's disease. *International journal of alzheimer disease*, 2012, 1–8.

Monge-Fuentes, V., *et al.*, 2021. Dopamine-loaded nanoparticle systems circumvent the blood–brain barrier restoring motor function in mouse model for Parkinson's disease. *Scientific reports*, 11 (1), 1–16.

Muntimadugu, E., *et al.*, 2016. Intranasal delivery of nanoparticle encapsulated tarenflurbil: A potential brain targeting strategy for Alzheimer's disease. *European journal of pharmaceutical sciences : official journal of the European federation for pharmaceutical sciences*, 92, 224–234.

Nikalje, A. P., 2015. Nanotechnology and its applications in medicine. In: W. Wang and S.A. Soper, eds. *Bio-MEMS Technologies and Applications*. CRC Press, Taylor and Francis Group, London, 81–89.

Nordberg, A., 1996. Functional studies of new drugs for the treatment of Alzheimer's disease. *Acta neurologica Scandinavica*, 94 (S165), 137–144.

Sharma, S., *et al.*, 2020. Multi-spectroscopic monitoring of molecular ionic liquid and potential anti-Alzheimer's drugs. *RSC advances*, 10 (64), 38873–38883.

Rajasekhar Reddy, A., *et al.*, 2018. Effect of catalyst and solvent in synthesis of tacrine-terpenoid hybrid analogues : friedlander annulation approach. *Journal of chemical and pharmaceutical sciences*, 11 (04), 293–301.

Lokhande, M.V., Kumar Gupta, M., and Rathod, N.G., 2013. Structural elucidation of process-related impurity in memantine hydrochloride bulk drug by GCMS, NMR and IR techniques. *International journal of medicine and pharmaceutical sciences*, 3 (3), 107–114.

Ribovski, L., Hamelmann, N.M., and Paulusse, J.M.J., 2021. Polymeric nanoparticles properties and brain delivery. *Pharmaceutics*, 13 (12), 2045.

Romero, A., and Marco-Contelles, J., 2017. Recent developments on multi-target-directed tacrine for Alzheimer's disease. I. The pyranotacrines. *Current topics in medicinal chemistry*, 17 (31), 3328–3335.

Romero, A., *et al.*, 2013. Novel tacrine-related drugs as potential candidates for the treatment of Alzheimer's disease. *Bioorganic & medicinal chemistry letters*, 23 (7), 1916–1922.

Ríos, D.L., *et al.*, 2019. Tacrines for Alzheimer's disease therapy III. *The pyridotacrines. European journal of medicinal chemistry*, 166, 381–389.

Sadeghi, F., *et al.*, 2020. Synthesis of a novel PEGylated colon-specific azo-based 4-aminosalicylic acid prodrug. *Iranian journal of basic medical sciences*, 23 (6), 781–787.

Sarathlal, K.C., *et al.*, 2021. Exploring the neuroprotective potential of rosiglitazone embedded nanocarrier system on streptozotocin-induced mice model of Alzheimer's disease. *Neurotoxicity research*, 39 (2), 240–255.

Silva-Abreu, M., *et al.*, 2018. PPARγ agonist-loaded PLGA-PEG nanocarriers as a potential treatment for Alzheimer's disease: In vitro and in vivo studies. *International journal of nanomedicine*, 13, 5577–5590.

Singh, A., *et al.*, 2015. Preparation and characterization of rizatriptan benzoate loaded solid lipid nanoparticles for brain targeting. *Materials today: proceedings*, 2 (9), 4521–4543.

Singh, A.P., *et al.*, 2019. Targeted therapy in chronic diseases using nanomaterial-based drug delivery vehicles. *Signal transduction and targeted therapy*, 4 (1), 1–21.

Summers, W.K. Tacrine in the treatment of Alzheimer's disease. https://jpands.org/hacienda/article31.html. (Accessed 18 May 2022).

Sun, M., *et al.*, 2017. Synthesis and characterization of hyperbranched poly(ester-amine) by Michael addition polymerization. *Designed monomers and polymers*, 20 (1), 458–467.

Tariot, P.N., *et al.*, 2004. Memantine treatment in patients with moderate to severe Alzheimer disease already receiving donepezil: a randomized controlled trial. *Journal of the American medical association*, 291 (3), 317–324.

Machtakova, M., Thérien-Aubin, H., and Landfester, K., 2022. Polymer nano-systems for the encapsulation and delivery of active biomacromolecular therapeutic agents. *Chemical society reviews*, 51 (1), 128–152.

Vecchio, I., *et al.*, 2021. The state of the art on acetylcholinesterase inhibitors in the treatment of Alzheimer's disease. *Journal of Central nervous system disease*, 13, 1–13.

Wu, I.Y., *et al.*, 2019. Interpreting non-linear drug diffusion data: utilizing the Korsmeyer-Peppas model to study drug release from liposomes. *European journal of pharmaceutical sciences : official journal of the European federation for pharmaceutical sciences*, 138, 105026.

Youssif, K.A., *et al.*, 2019. Anti-Alzheimer potential, metabolomic profiling and molecular docking of green synthesized silver nanoparticles of Lampranthus coccineus and Malephora lutea aqueous extracts. *PLOS one*, 14 (11), e0223781–19.

Zhang X., and Tian, Y., *et al.*, 2021a. The epidemiology of Alzheimer's disease modifiable risk factors and prevention. *The journal of prevention of Alzheimer's disease*, 8 (3), 313–321.

Zhang, W., *et al.*, 2021b. Carbon dots: a future blood–brain barrier penetrating nanomedicine and drug nanocarrier. *International journal of nanomedicine*, 16, 5003–5016.

Zeeshan, M., *et al.*, 2019. Nanopharmaceuticals: a boon to the brain-targeted drug delivery', in U. Ahmad, J. Akhtar (eds.), *Pharmaceutical Formulation Design – Recent Practices*, IntechOpen, London.

Zhao, B., *et al.*, 2019. Synthesis and characterization of novel porphyrin-cinnamic acid conjugates. *Spectrochimica acta. Part A, molecular and biomolecular spectroscopy*, 223, 117314.